INTERNATIONAL JOURNAL OF PRECISION ENGINEERING AND MANUFACTURING-GREEN TECHNOLOGY Vol. 3, No. 1, pp. 27-34 JANUARY 2016 / 27
DOI: 10.1007/s40684-016-0004-8 ISSN 2288-6206 (Print) / ISSN 2198-0810 (Online)

Establishment and Analysis of Erosion Depth Model for Impeller Material FV520B

Zi-Wu Liu[1], Jian-Feng Li[1,#], Xiu-Jie Jia[1], Guang-Cun Wang[1], and Wen-Han Xu[1]

1 School of Mechanical Engineering, Shandon University, 5-4, Jingshi-road, Jinan, Shandong, 250061, China
Corresponding Author / Email: ljf@sdu.edu.cn, TEL: +86-0531-88392003, FAX: +86-0531-88392058

KEYWORDS: Orthogonal experiment, Surface morphology, Erosion depth model, Particle impact, Impeller material, Life evaluation

The multifactorial erosion was conducted in this paper to test the compressor impeller material FV520B using high-speed gas-solid two phase flow erosion tester and surface morphology analysis method. Based on the particle motion and collision energy equation as well as regression analysis of multi-factor orthogonal experiment, a phenomenological erosion depth model which captures the effects of impact velocity, angle and particle size, has been developed. The model includes removal of material due to both deformation damage and micro-cutting. Results show that the peak of experiment depth and the maximum calculated depth all appeared at near 45°, rather than near 24° where the maximum erosion rate appeared. Comparing the calculated values and the results of each single factor experiment, the errors are within 15%. The predictions of the simplified version of the model were in good agreement with the results of single factor experiments. Also, the reliability of the assessment formula was verified to assess the impeller erosion life, which indicated that this calculation model could be used to estimate the erosion depth of compressor impeller material FV520B.

Manuscript received: April 15, 2015 / Revised: November 2, 2015 / Accepted: November 13, 2015
This paper was presented at ISGMA2015

1. Introduction

The air compressor is the core equipment of petrochemical industry, and is commonly used in industrial area.[1,2] Being the main component of a compressor, the impeller's rotation speed can reach 2000 r·min^{-1}-100000 r·min^{-1}. Due to the existence of solid particles (industrial dust, coal powder, organic particles, and secondary particles) in the transport medium, the impeller suffers solid particle erosion seriously. Impacting particles can form foveolate furrows on the blade surface, which would cause the blade fractured. The mechanism of blade fracture is reported as follows: a defect forms foveolate furrows (erosion pit) and a crack is initiated and propagated from the defect under high cycle fatigue (HCF).[3] Generally, when erosion depth reaches a certain value, the efficiency of the leaf level will fall by more than 3%.[4] In order to understand the erosion process deeply, the erosion behaviors of metals, coatings nonmetals (glass, etc.), and even polymer materials (rubber, etc.) have been studied by many literatures.[5-9] But erosion depth model is also not established.

Extended life is one way of effective utilization of resources and increasing resource productivity.[10] To reduce the impeller erosion wear and predict its residual life for remanufacturing, based on BITTER's deformation and wear theory, a new erosion model-erosion depth model for plastic metal is developed. By measuring the contour of the erosion pit, erosion depth of impeller material FV520B is got accurately. A series of erosion tests for FV520B has been conducted to verify the erosion depth calculation model. At last, we evaluate a type of impeller thinning life.

2. Mechanism Model for Erosion Depth

According to BITTER's deformation and wear theory,[11] the erosion mechanism of plastic metals is the combination of micro-cutting and deformation wear. The total loss consists of these two parts. It can be expressed as:

$$W_e = W_d + W_c \tag{1}$$

Where W_e is the total loss; W_d, W_c are the losses by deformation wear and cutting wear, respectively. There are many factors in a pure erosion. The functional relationship can be expressed as:

$$W_e = f(V, \theta, d_P, S_P, \rho_P, H_P, E_P, H_O, E_O, \sigma_O, \ldots) \quad (2)$$

Where V, θ, d_P, S_P, ρ_P, H_P and E_P are particle's impact velocity, impact angle, size, shape, density, hardness and elasticity modulus, respectively; H_O E_O and σ_O are the hardness, elasticity modulus and flow stress of the target, and σ_O can be described by Johnson-cook constitutive model.

When the particle impacts the target at a certain angle and speed, the impact velocity can be decomposed into normal velocity and tangential velocity. These two velocity components produce a normal and a tangential force. These two forces play different roles in the erosion process. Normal force impacts the target surface acting as a hammer, and produces lots of tips and lips. With the continuous impact of normal force, the lips fall off the surface like debris because of undergoing severe plastic deformation, which is called deformation wear.

If the particle is sharp, the tangential force scratches across the target surface acting as a tool and cuts down material as chips, which is called micro-cutting. But if the particle is not sharp enough, the tangential force scratches across the target surface like a plow, and leaves furrow and hump, which is named plowing. The hump around the furrow will be removed by subsequent particles. In this paper, micro-cutting and plowing are collectively called as cutting wear.

Thus cutting wear can be regarded as a function of the tangential velocity, while deformation wear can be regarded as a function of the normal velocity, and the total erosion is the sum of them.

For simplicity, the following assumptions are made. Firstly, the single particle's shape is spherical. Secondly, the particle's hardness is larger than the target material's hardness, so that the deformation of the particle during the impact process is negligible. Thirdly, the indentation's depth is smaller than the particle's size. Finally, in fact, because most particles are polygonal, the shape of the particles will be taken into account in later analysis.

2.1 Removal of Material due to Plastic Deformation

Fig. 1 shows the schematic diagram of the normal impact. According to the assumptions, the area of the indentation can be expressed as:

$$A_y \approx \pi y d_P \quad (3)$$

Where y is the depth of the indentation; d_p is the particle's diameter. For simplicity, the contact force formula given by Sheldon and Kanhere is adopted:

$$F_y = \frac{1}{4}\pi \sigma_n D^2 \quad (4)$$

Where D is the width of the indentation on the target surface; σ_n is the constant pressure of the target (for the Vickers Hardness, it can be described as $\sigma_n = H_V/(0.102)$). According to Fig. 1, D can be expressed as:

$$D = 2[d_p y - y^2]^{1/2} \quad (5)$$

The particle's initial kinetic energy E_1 can be expressed as:

$$E_1 = \frac{1}{2} m V_y^2 = \frac{1}{12}\pi \rho_p d_p^3 V_y^2 \quad (6)$$

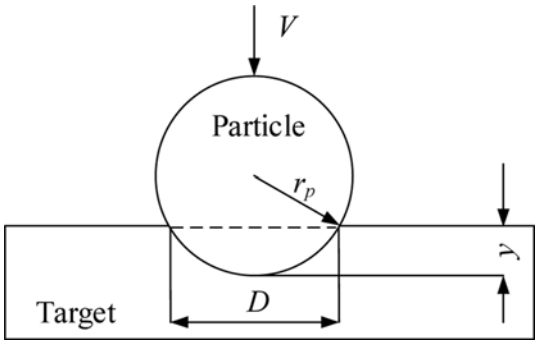

Fig. 1 Schematic diagram of normal impact

Where V_y is the component of particle's impacting velocity in normal direction; ρ_p is the particle's density. During the entire process of impact, according to energy conservation, it can be expressed as:

$$E_2 = \int_0^{y_{\max}} F_y dy \quad (7)$$

Where $y_{\max}$ is the maximum depth of the indentation. Assuming that, all the kinetic energy of the particle is used to cause the target plastic deformation, namely, $E_1 = E_2$. The maximum depth and width of the indentation can be respectively expressed as:

$$y_{\max} = \frac{d_p \rho_p^{1/2} V_{y0}}{(6\sigma_n)^{1/2}} \quad (8)$$

$$D_{\max} = 2[d_p y - y^2]^{1/2} \approx \frac{2 d_p \rho_p^{1/4} V_{y0}^{1/2}}{(6\sigma_n)^{1/4}} \quad (9)$$

In the area of the indentation, considering the effect of particles' superimposition at the indentation center, the equivalent deformation depth can be expressed as:

$$y_d = \int_0^{y_{\max}} A_y dy = \int_0^{y_{\max}} \pi d_p y dy = \frac{\pi d_p^3 \rho_p V_{y0}^2}{12\sigma_n} \quad (10)$$

The deformation wear is an accumulation of plastic deformation of target material around indentation caused by the particle's vertical impact. The material removal depends not only on the properties of target such as hardness and work hardening, but also on the deformation volume which is related to the indentation volume. With Hutchings' method,[12] the critical strain ε_c and Coffin-Manson formula are used to calculate the deformation wear approximately, namely, $\varepsilon_c = 2\Delta\varepsilon N^b$ (N is the impact numbers at which the strain on the deformation area reaches ε_c leading to material removal from the target; $\Delta\varepsilon$ is the average strain caused by each impact; b is a function of material's properties determined by experiments). Then the deformation depth of each impact can be expressed by the following equation:

$$y_{ed} = y_d \left(\frac{2\Delta\varepsilon}{\varepsilon_c}\right)^{1/b} \quad (11)$$

According to D. Tabor empirical equation, one has:

$$\Delta\varepsilon \approx \frac{0.2D}{d_p} = \frac{0.4 \rho_p^{1/4} V_{y0}^{1/2}}{(6\sigma)^{1/4}} \quad (12)$$

The critical strain ε_c can be deduced by material's constitutive equation and adiabatic shear instability conditions.

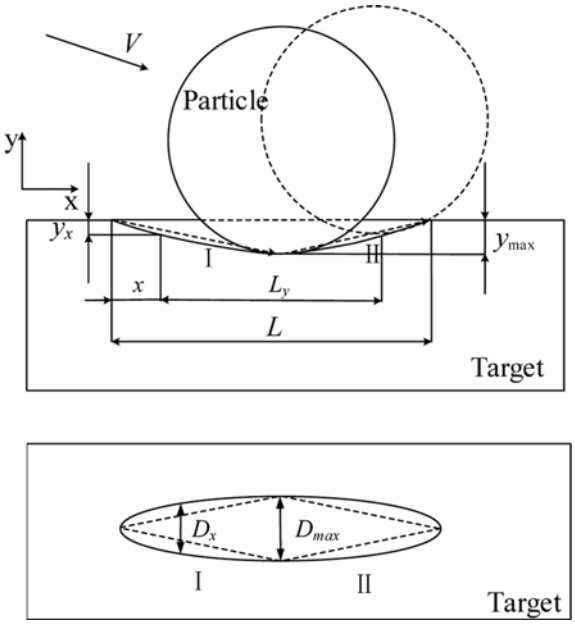

Fig. 2 The ideal pattern of micro-cutting wear

$$\varepsilon_c = \left(\frac{n\rho_t C_t}{3KT}\right)^{n/(n+1)} \tag{13}$$

Where C_t is the specific heat capacity of target, K is the strengthening coefficient, T is the temperature coefficient related to the shear modulus, n is the hardening index. Substituting (10) and (12) into (11), one has:

$$y_{ed} = c_1 \frac{d_p^3 \rho_p^{1+1/4b} V^{2+1/2b} (\sin\alpha)^{2+1/2b}}{\sigma_n^{1+1/4b} \varepsilon_c^{1/b}} \tag{14}$$

2.2 Removal of Material due to Cutting

Fig. 2 shows an ideal pattern. This process can be divided into two stages. Stage I: The article impacts the target at a certain angle with a certain speed. With the combination of normal and tangential forces, the cutting depth of particle increases until $y_{\max}$ is reached. Stage II: Under the effect of the resistance force from target, the cutting depth decreases, and the particle leaves from the surface at a certain angle with a certain speed after cutting down the other part of the material.

For simplicity, the following assumptions are made. Firstly, the shapes of two phases are equal. Secondly, the cutting trajectories of two phases are approximately linear. Thirdly, the removed material can approximate to a pyramid. In this figure, symbols y_x and D_x are cutting depth and width at x position; L_y is the length of the cutting cross-section at the cutting depth of y_x; L, y_{max} and D_{max} are the maximum cutting length, depth and width, respectively. The area of the cutting mark on the surface of the target can be calculated by following equation approximately:

$$A_x \approx LD_{\max} \tag{15}$$

$$y_x \approx 2xy_{\max}/L \quad x \in (0, L/2) \tag{16}$$

$$D_x \approx 2xD_{\max}/L \quad x \in (0, L/2) \tag{17}$$

In the area of the cutting mark, considering the effect of particles superimposition on the center of the cutting mark, the equivalent deformation depth can be expressed as:

$$y_{ec} = \int_0^{y_{\max}} \frac{L_y D_x dy_x}{2} = y_{\max} D_{\max} L/6 \tag{18}$$

In most cases, micro-cutting is caused by polygonal sharp particles. Then the cross-sectional area of the cutting mark is A. In the cutting process, tangential resistance of the particle can be expressed as:

$$F_x = c_3 A \sigma_\tau \tag{19}$$

Where c_3 is stress factor; σ_τ is the particle material flow stress in the process of cutting.

In Fig. 2, the ideal cross-sectional area of the cutting mark is ΔA_x. The particle is subjected to cutting resistance from the material, which is related to the properties of the material, the particle's edge shape and the rake angle in the micro-cutting process. Considering this, the particle shape factor g is adopted, namely, $A = \Delta A_x^g$. It is associated with particle's edge shape and the rake angle in the micro-cutting process. It represents the degree of difficulty for one particle to cut down a certain volume of material from the target, and the smaller the value is, the easier the micro-cutting process is. Thus the micro-cutting resistance can be expressed by the following equation approximately:

$$F_x = c_3 \Delta A_x^g \sigma_t \tag{20}$$

When the particles remove the material from the surface of the target, energy consumption is equal to the decrease of particle's kinetic energy. The energy equation is:

$$2\int_0^{L/2} F_x dx = \frac{1}{2} m(V_{x0}^2 - V_{xout}^2) \tag{21}$$

Where V_{xout} is the tangential velocity when the particle leaves the target surface. For simplicity, we assume that, $V_{xout} = c_4 V_{x0}$, where c_4 is a coefficient, and $c_4 \le 1$. If the flow stress σ_t does not change and particle is not broken while cutting, Substituting (19) and (20) into Eq. (21) and integrating it, we have:

$$L = \frac{c_5 m V_{x0}^2}{y_{\max}^g D_{\max}^g \sigma_t} \tag{22}$$

Where $c_5 = (1c_4^2)(2g + 1)/(2c_3)$. Substituting (8), (9) and (22) into (18), one has:

$$y_{ec} = \frac{c_6 d_p^{5-2g} \rho_p^{(7-3g)/4} V^{2+3(1-g)/2} (\sin\alpha)^{3(1-g)/2} (\cos\alpha)^2}{\sigma_n^{3(1-g)/4} \sigma_t} \tag{23}$$

2.3 Calculation Model of Erosion Depth

According to Fig. 3, in unit time and unit normal section area, when particles impact target at a certain mass flow of Q, a certain mass concentration of P ($Q = Pv$) and angle of α, the total numbers of particles impacting the unit area of the target surface are N. It can get: $N = 6Qd_p^{-3}\rho_p^{-1} \sin\alpha/\pi$. In unit time, if the numbers of particles impacting point of surface are n, namely, $n = c_7 N$, where c_7 is the

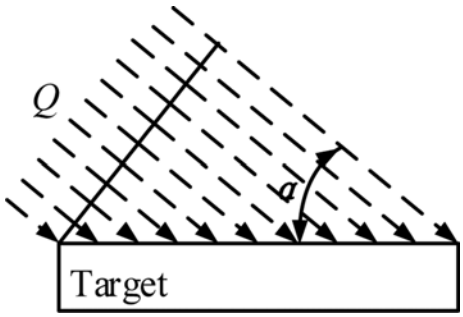

Fig. 3 Sketch of multiparticle impacting on the target

number factor of the particle and a parameter related to particle's size. When erosion time is t, the erosion depth can be expressed as:

$$Y_d = nt(y_{ed}+y_{ec}) = \frac{6c_7Qt}{\pi}\left(\frac{c_2\rho_p^{1/4b}V^{2+1/2b}(\sin\alpha)^{3+1/2b}}{\sigma_n^{1+1/4b}\varepsilon_c^{1/b}}\right. \quad (24)$$

$$\left.+\frac{c_6d_p^{2-2g}\rho_p^{(3-3g)/4}V^{2+3(1-g)/2}(\sin\alpha)^{(5-3g)/2}(\cos\alpha)^2}{\sigma_n^{3(1-g)/4}\sigma_t}\right)$$

For a specific material and in specific erosion condition, properties of both target and particle are constant, and treated as coefficients. Then we have:

$$Y_d = Qt(F_1\rho_p^{1/4b}V^{2+1/2b}(\sin\alpha)^{3+1/2b} + F_2d_p^{2-2g}\rho_p^{(3-3g)/4}V^{2+3(1-g)/2}(\sin\alpha)^{(5-3g)/2}(\cos\alpha)^2) \quad (25)$$

This equation includes the effect of particle's shape, size, velocity, time and impact angle of particle. All coefficients and exponents must be determined from the experiments.

3. Experiment and Model Validation

3.1 Erosion Experiment Device

The erosion experiment was tested by the gas-solid two-phase flow test machine at Xi'an Jiaotong University. The velocity, impact angle and dosage of particle could be controlled.[13]

3.2 Experimental Material

FV520B is an ideal material to produce centrifugal compressor impeller, with high corrosion resistance, strength and hardness. Provided by Shenyang Blower Factory, chemical composition is shown in Table 1; the heat treatment technology is shown in Table 2; the mechanical properties are shown in Table 3.

3.3 The Characteristics of Erosion Particle Analysis

Impact particle: The work medium of centrifugal air compressor was industrial atmosphere, so polygonal alumina particles with diameters of 7 μm, 10 μm and 14 μm ≤ were chosen to be the impact particles. Different particle sizes were obtained by flotation method.

Particle concentration: using uniform flow to adding particles, stability and continuity of feeding could be implemented.[11] Using indirect measurement, we got the feed concentration between 2.05-3.07 g/m^3 at different impact speeds. Although particles' interaction would affect the results of erosion, according to the literature,[14,15] when the concentration of particles was not more than 100 g/m^3, the influence of particles' interaction would be ignored, and could be treated as the lean phase.

Table 1 Chemical components of FV520B

Chemical components and mass fractions / %				
C	Mn	Si	Cr	Ni
0.03	0.41	0.30	14.51	5.24
Mo	Nb	Cu	S	P
1.95	0.65	1.54	≤0.025	≤0.03

Table 2 Heat treatment technology of FV520B

Solid solution °C × h	Over aging °C × h	Releasing stress °C × h	Quenching °C × h	Tempering °C × h
1050×1.5	630×4	640×5	850×3.5	470×5

Table 3 Physical and mechanical properties of FV520B

Yield strength MPa	Tensile strength MPa	Elongation %	Reduction of area %	Surface hardness HV
1182	1229	14.3	61.3	300

Particle velocity: The speed of particle could be measured by Particle Image Velocimetry (PIV). Because the particle inertia was large and flow boundary layer was very thin, the effect on the particle motion was very small. The particle velocity which was measured nearly 0.5 mm away from the wall could be approximated to the impact velocity of the particle.

Impact angle of particle: Slip between the particles and airflow formed the aerodynamic conditions of the erosion. Particle deviated from the airflow direction. At the same time, particle impacted the blade surface with larger speed. Generally the impact angle was between 20°-40°.[16] So the erosion angles were chosen with 12°, 18°, 24°, 30°, 36°, 45°, 60°, 75° and 90°.

Erosion test process: When tested, the specimen was mounted on the sample-holding device with a certain angle to the central line of nozzle. The high-speed air mixed with the impact particles was jetted from the nozzle (the nozzle diameter was 10 mm), and impacted the surface of the target to produce erosion wear. Feed rate was controlled at 2.5 g/min. So the particle mass flow was 530.5 μg/s per square millimeter. According to the former researches, when the particle mass exceeded 80 g, the erosion stage came into stable period. The mass of the target was measured before and after the test with an analytical balance with accuracy of 0.1 mg to calculate erosion rate. The outline of the erosion pit was measured by Veeco NT9300 white light interferometer, and the depth of the erosion was expressed as the maximum distance between the original surface and the erosion surface.

3.4 Test Results and Analysis

The three-factor and three-level orthogonal experiment was designed including impact velocity, impact angle and particle diameter, when t = 40 min. The constant parameters (F_1, F_2, b, g) in the erosion

Table 4 Design and results of orthogonal experiment

Test No.	Impact velocity m·s^{-1}	Impact angle °	Particle diameter μm	Test depth μm	Calculated data μm	Error %
1	120	12	7	12.82	13.32	0.039
2	120	36	10	46.12	43.43	0.058
3	120	60	14	44.81	38.85	0.133
4	150	12	10	24.67	25.84	0.047
5	150	36	14	96.93	83.16	0.140
6	150	60	7	55.24	53.04	0.040
7	180	12	14	51.24	45.24	0.120
8	180	36	7	97.04	96.80	0.002
9	180	60	10	86.43	90.64	0.049

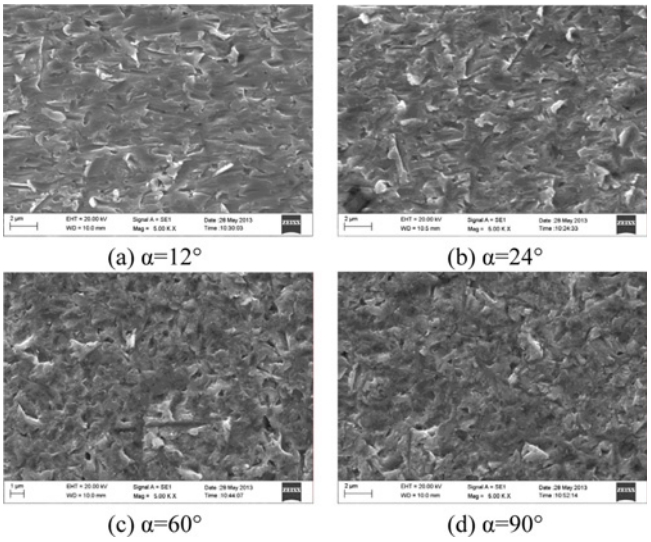

Fig. 4 SEM micrographs of the erosion surface

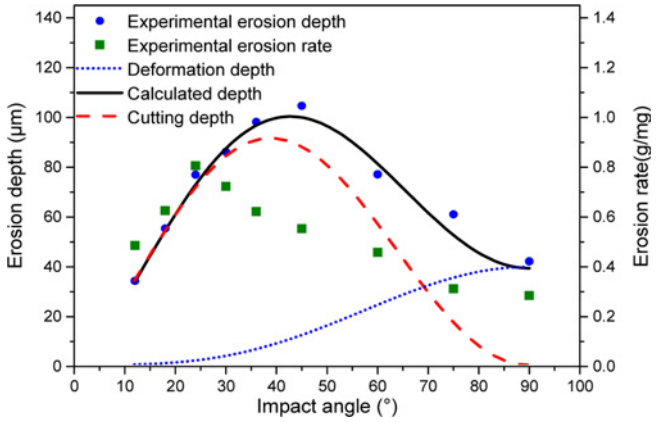

Fig. 5 Comparison of calculated erosion depth with experimental

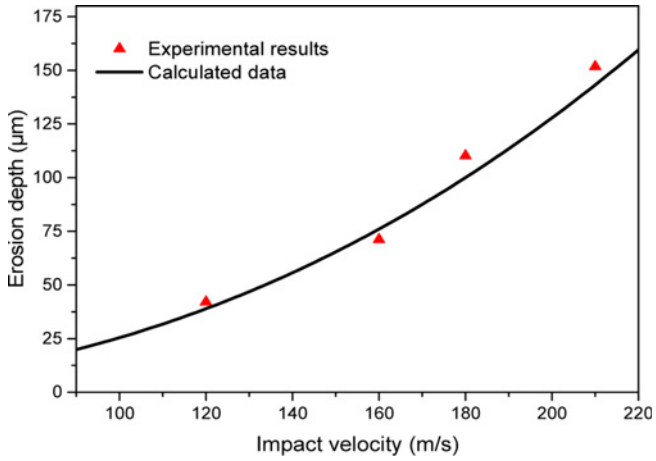

Fig. 6 Effect of velocity on erosion depth

depth model were solved by use of the regression analysis method. Orthogonal table design and test results are shown in Table 4.

According to results of orthogonal experiment, the constant parameters were determined by nonlinear regression analysis based on Origin Pro 9.1. The formula of erosion depth model can be expressed as:

$$Y_d = 6.234E-4 \times Qt\rho_p^{0.2325} V^{2.4650} (\sin\alpha)^{3.4650} + 4.855E-4 \times Qtd_p^{0.4140} \rho_p^{0.1552} V^{2.3105} (\sin\alpha)^{1.3105} (\sin\alpha)^2 \quad (26)$$

From the study, we find determination coefficients R^2 is 0.979, namely, correlation coefficient $r = 0.9895$. It is mean that there are high coherence between the setting coefficient and erosion depth. Comparing the calculated values and the results of orthogonal experiment, the errors are within 10% except three errors within 15%. The equation indicates that the exponent of impact velocity is 2.3105 at cutting erosion which is consistent with the exponent range of 2.2-2.4 at low angle.[17,18] The exponent of impact velocity is 2.4650 at deformation erosion which is less than the exponent of 2.55 at positive impacting.[19] The good agreement between the predictions and the experiments shows that this simplified model is reasonable and useful.

We verified the depth model using single factor erosion experiment. Fig. 4 shows the SEM micrographs of the erosion surface and Fig. 5 shows comparison between the experiment depths and the calculated depths, when time is 40 min; particle size is 7 μm, impact velocity is 180 m/s and at different impact angles. Fig. 4 shows the obvious differences at different impact angles: at attack angle of 12°, Fig. 4(a) shows obvious morphology of cutting grooves and plough lips; at attack angle of 24°, Fig. 4(b) shows that the cutting marks on the surface become fewer and shorter, and plough marks become more and darker with a few of pits and material lips; at attack angle of 60°, Fig. 4(c) shows that erosion main morphology is pits of lateral hammer and material lips, besides a few of deeper revolution marks; at attack angle 90°, Fig. 4(d) shows that erosion morphologies are different depths of hemp dot pits, material lips and flaking wear debris.[20,21] Fig. 5 shows that, both experiment depths and calculated depths have the same changing trend with the impact angle. The peaks of experiment depth and the maximum calculated depth all appear on near 45°, but the peak of erosion rate appears on near 24°. At high angle the impact depth is deeper, but at low angle the cutting line is longer; and at one certain point the depth is formed by the action of the particles superimposition.

Fig. 6 shows the comparison between the experiment depth and the calculated depth, when time is 4 min; particle size is 7 μm, impact angle is 45° and at different impact velocity. Erosion depth has an approximate exponential relationship with impact velocity. The errors are within 10%.

Fig. 7 shows the comparison between experiment depths and calculated depths, when time is 4 min; impact velocity is 180 m/s, impact

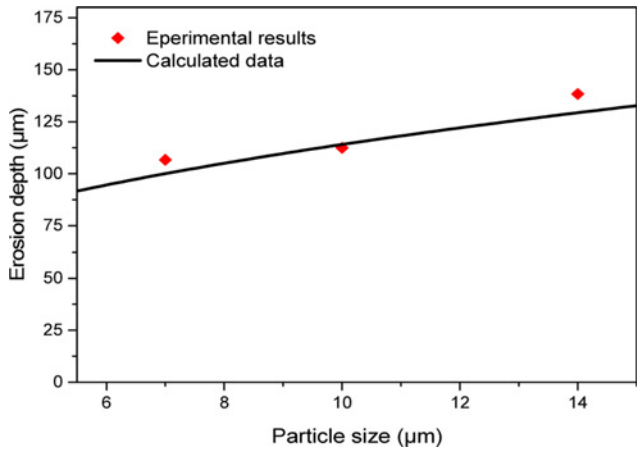

Fig. 7 Effect of particle size on erosion depth

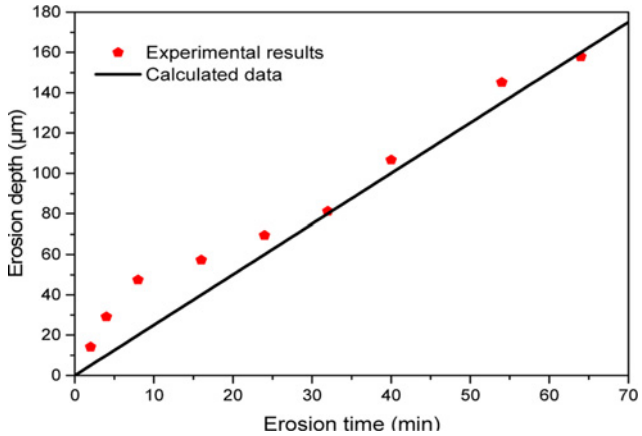

Fig. 8 Effect of velocity on erosion time

angle is 45° and at different particle size. The test results achieve high conformity with the calculation model. The errors are within 10%.

Fig. 8 shows the comparison between the experiment depths and the calculated depths, when particle size is 7 μm; impact velocity was 180 m/s, impact angle is 45° and at different erosion time. From 0-32min, errors are more than 15%, because this period is induction period. After induction period, the test other errors are within 10%.

4. Blade Life Evaluation

In 2012, a type of air separation compressor impeller of Shenyang Blower Group which run two years later, was overhauled. The area of blade leading edge was not obviously thinning, but the area of large blade pressure surface trailing edge was seriously erosion thinning, and the maximum erosion depth was up to 7mm (the original thickness of the blade was 8 mm). The erosion thinning impeller is shown in Fig. 9. The working condition of compressor is shown as:

Strainer element accuracy: 10 μm
Annual average PM10 concentrations: 168 μg/m^3
Annual average PM2.5concentrations: 86 μg/m^3
Outlet diameter: 918 mm
Revolving speed: 6180 r/min
Inlet pressure: 170 kPa
Quantity of flow: 26 kg/s

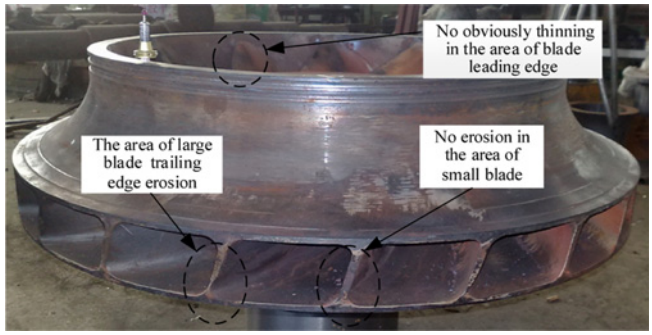

Fig. 9 Erosion thinning in air separation compressor impeller

Fig. 10 3D model of impeller and the flow channel

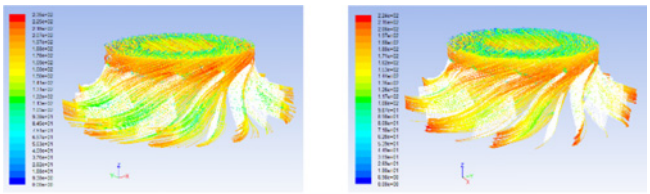

Fig. 11 Particle trajectories and relative velocity

According to the large and small impeller blade profile data, impeller disc and impeller cover meridian plane provided by Shenyang Blower Works, 3D models of impeller and flow channel were founded by software of PRO/E which are shown as Fig. 10.

The two sets of tests were designed with the particle diameters of 5 μm and 10 μm respectively, and particle concentration was set as 0.0002 kg/m^3. Each group 5112 particles moving trajectories were tracked and they were shown as Fig. 11.

Fig. 11 shows that vast majority of particles enriches at the area of large blade pressure surface and outflows from the area of large blade pressure surface trailing edge. It conforms to the phenomenon of impeller erosion. The particles relative velocities in the area of large blade pressure surface trailing edge are between 150-180 m/s. The typical moving trajectory of particles are extracted, and the impact angle at the pressure surface trailing edge is about 25°.

Fig. 12 shows the concentration distribution of the large blade pressure surface. We can find that average enrichment factor of particle concentration is about 180 times.

When particles are smaller than 3 μm, particles easily scales and deposits on blade pressure surface.[22] So these particles erosion effect

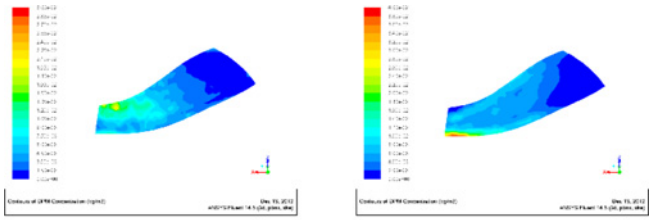

(a) Particle size = 5μm (b) Particle size = 10μm

Fig. 12 Concentration of particles at large blade pressure surface

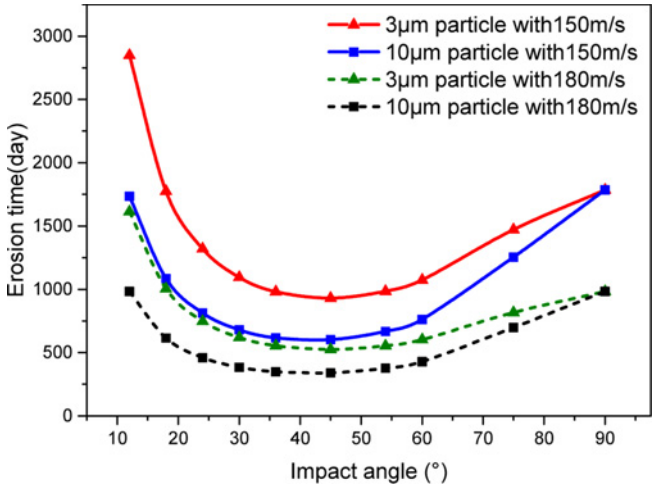

Fig. 13 Life curve of the blade thinning 7 mm

could be ignored. The particle diameter ranges from 3 μm to 10 μm, and impact velocity ranges from 150 m/s to 180 m/s. Combing above analysis, the above data are substituted into the Eq. (26). We can get the relationship between erosion times and impact angles plotted in Fig. 12.

Fig. 13 shows that the relation of thinning life of leaf blade and impact angle is U-shaped at different particle size and velocity. The blade is thinned 7 mm in 730 days, and this result is between the upper limit and the lower limit at the angle of about 25°. It shows agreement with the calculation at particle size of 10 μm and impact velocity of 150 m/s or at particle size of 3 μm and impact velocity of 180 m/s. The calculation formula of blade thinning life is proved relatively accurate.

5. Conclusions

A new erosion depth model, which captures the effects of the impact velocity, angle, time of erosion shape properties of target and particle, is established by orthogonal fitting in a simulated environment. Variance analysis showed that the formula is very significant. The exponent of impact velocity ranging is consistent to experimental findings. For the exponent of siná, it depends on the particle's shape. Moreover, the particle size plays an important role in the model of cutting removal. Compared with the results of each single factor experiment, the formula could predict the erosion depth of FV520B. At last, the erosion depth model is good agreement with the erosion thinning of the certain type of compressor impeller provided by Shenyang Blower Group.

ACKNOWLEDGEMENT

The authors would like to thank the National Key Basic Research Program of China (No. 2011CB013400) and the National High Technology Research and Development Program of China (No. 2013AA040204) support. The authors would also particularly like to thank Mr. Wang Shun-sen of the Xian Jiaotong University for their ongoing supportive interest in this work.

REFERENCES

1. Utamura, M., Fukuda, T., and Aritomi, M., "Aerodynamic Characteristics of a Centrifugal Compressor Working in Supercritical Carbon Dioxide," Energy Procedia, Vol. 14, pp. 1149-1155, 2012.
2. Dowson, P., Walker, M. S., and Watson, A. P., "Development of Abradable and Rub-Tolerant Seal Materials for Application in Centrifugal Compressors and Steam Turbines," Sealing Technology, Vol. 2004, No. 12, pp. 5-10, 2004.
3. Yoon, W. N., Kang, M. S., Jung, N. K., Kim, J. S., and Choi, B.-H., "Failure Analysis of the Defect-Induced Blade Damage of a Compressor in the Gas Turbine of a Cogeneration Plant," Int. J. Precis. Eng. Manuf., Vol. 13, No. 5, pp. 717-722, 2012.
4. Kawagishi, H., Kawassaki, S., and Ikeda, K., "Protective Design and Boride Coating Against Sol Id Particle Erosion of First Stage Turbine Nozzles," Advances in Steam Turbine Technology for Power Generation, Vol. 1990, No. 10, pp. 23-29, 1990.
5. Parsi, M., Najmi, K., Najafifard, F., Hassani, S., McLaury, B. S., et al., "A Comprehensive Review of Solid Particle Erosion Modeling for Oil and Gas Wells and Pipelines Applications," Journal of Natural Gas Science and Engineering, Vol. 21, pp. 850-873, 2014.
6. Mbabazi, J., Sheer, T., and Shandu, R., "A Model to Predict Erosion on Mild Steel Surfaces Impacted by Boiler Fly Ash Particles," Wear, Vol. 257, No. 5, pp. 612-624, 2004.
7. Duan, X.-M., Jia, D.-C., Zhou, Y., Yang, Z.-H., Wang, Y.-J., et al., Mechanical Properties and Plasma Erosion Resistance of BNp/Al_2O_3-SiO_2 Composite Ceramics, Journal of Central South University, Vol. 20, No. 6, pp. 1462-1468, 2013.
8. Kim, W.-B., Nam, E., Min, B.-K., Choi, D.-S., Je, T.-J., et al., "Material Removal of Glass by Magnetorheological Fluid Jet," Int. J. Precis. Eng. Manuf., Vol. 16, No. 4, pp. 629-637, 2015.
9. Hu, Y., Kang, Y., Wang, X.-C., Li, X.-H., Long, X.-P., et al., "Mechanism and Experimental Investigation of Ultra High Pressure Water Jet on Rubber Cutting," Int. J. Precis. Eng. Manuf., Vol. 15, No. 9, pp. 1973-1978, 2014.
10. Dornfeld, D. A., "Moving towards Green and Sustainable Manufacturing," Int. J. Precis. Eng. Manuf.-Green Tech., Vol. 1, No. 1, pp. 63-66, 2014.
11. Bitter, J. G. A., "A Study of Erosion Phenomena," Wear, Vol. 6, No. 1, pp. 5-21, 1963.

12. Hutchings, I. M., "A Model for the Erosion of Metals by Spherical Particles at Normal Incidence," Wear, Vol. 70, No. 3, pp. 269-281, 1981.

13. Wang, S.-S., Liu, G.-W., Mao, J.-R., Guo, H., Ma, X., et al., "Modeling Experimental System for Solid Particle Erosion on the Steam Turbine Nozzle Blades and Measuring Methods, Proc. of the Chinese Society of Electrical Engineering," Vol. 27, No. 11, pp. 103-108, 2007.

14. Cen, K. F., "The Theory and Computation of Gas-Solid Multiphase Flow in Engineering," Zhejiang: Zhejiang University Press, pp. 303-375, 1990.

15. Li, Z., "Similarity and Modeling (Theory and Application)," National Defence Industry Press, 1982.

16. Lu, J. H. and Ling, Z. G., "Numerical Analysis and Experiment Investigation of Blade Erosion in Particle-Laden Gas Turbine, Power Engineering," Vol. 22, No. 4, pp. 1858-1862, 2002.

17. Finnie, I. and McFadden, D. H., "On the Velocity Dependence of the Erosion of Ductile Metals by Solid Particles at Low Angles of Incidence, Wear," Vol. 48, No. 1, pp. 181-190, 1978.

18. Hutchings, I. M., "Corrosion/Erosion of Coal Conversion System Materials," Proc. of the Corrosion-Erosion of Coal Conversion System Materials, p. 393, 1979.

19. Brach, R. M., "Impact Dynamics with Applications to Solid Particle Erosion," International Journal of Impact Engineering, Vol. 7, No. 1, pp. 37-53, 1988.

20. Gu, Y., Chen, C. H., Chen, J. J., and Ye, X. C., "Research on Wear Behavior of 26Cr12Ni and 25Cr20Ni Stainless Steel," Hot Working Technology, Vol. 43, No. 8, pp. 84-86, 2014.

21. Yìldìzlì, K., Karamìs, M. B., and Nair, F., "Erosion Mechanisms of Nodular and Gray Cast Irons at Different Impact Angles," Wear, Vol. 261, No. 5-6, pp. 622-633, 2006.

22. Du, Y. P., Zhao, H., Yang, C. H., Zhang Y., and Hu, R., "Catalyst Fines Behavior among FCC Flue Gas Turbine Blade Rows-Erosion and Fouling on Blades," Chemical Engineering, Vol. 40, No. 9, pp. 52-55, 2012.